Analysis of solid blends milling using population balances.

Alejandro Barrientos Osorio[a] , Alejandro Echeverri Grajales[a],

Santiago Builes Toro[b]

[a] *Process Engineering Student, Universidad EAFIT, Medellín, Colombia*
[b] *Professor, Graduation Project Advisor, Process Engineering Department, Universidad EAFIT, Medellín, Colombia*

Abstract

Particle size distribution (PSD) is a key factor in size reduction processes. These processes are widely used worldwide and in the Colombian industry. However, they represent a high energy consumption process, which requires a careful assessment of the desired particle size and the energy required to obtain it. In order to reduce the capital costs, it is common for some companies to operate grinding stages with blends, reducing the capital costs and time required for the process. However, the blend composition can affect the operating conditions or require a higher energy consumption than grinding the individual components. Population balance modeling (PBM) can be used to describe the rate at which a material is being ground, and therefore, predict the time and energy required to obtain a desired PSD. In this work, the grinding behavior of two different materials and their blend in a batch size reduction process using a laboratory-scale steel ball mill was studied. The operating conditions were kept constant in order to study the evolution of PSD with time. The results obtained showed a good correlation between PSD and time using PBM for the pure materials. The blend could not be explained by a linear combination of the parameters. Further work is necessary to study blends in milling processes. It was also possible to determine the effect of grinding media size and mill filling in the rate of breakage of solids. However, the applicability of the model was only adequate for the coarser sizes of the samples, as shown by validation experiments.

1. Introduction

Many industrial processes worldwide include size reduction stages of solid materials, such as cement production, pigments, mining, food processing, agricultural processes and chemical industries, for: (i) conditioning raw materials, (ii) producing final products in powder, (iii) increasing surface area for reactions or separations, or (iv) easing waste disposal [1]. Some of these industries have a large share in the Colombian GDP, mainly mining and cement industries [2]. Size reduction processes require large amounts of energy. For instance, estimations on mine sites have shown that 53% of the total energy consumed corresponds to grinding processes[3]. Grinding energy consumption in the U.S. was estimated at 17.6 TWh in 2005, which corresponded to ~2% of the total industrial energy consumption [4]. Therefore, a careful design of equipment in order to minimize energy consumption is required.

Particle Size Distribution (PSD) is the dominant quality factor for products of size reduction stages. It defines the expected performance of a product in a given application [5]. Raw materials or final products, such as pigments or cement, must have fine particle sizes for their use, whereas solid waste does not require small particle sizes for its disposal. Consequently, comminution processes must have an adequate design so that energy consumption is adjusted to the requirements of the process. However, despite its importance, equipment design for size reduction unit operations is still made based on models that relate energy consumption with a single value of particle size, such as the Bond equation [6], without taking into account the whole distribution of sizes. This is because of the difficulty of describing or analyzing the forces acting on every single particle. Adequate equipment design for comminution must yield the desired PSD with the operating conditions and equipment required [1]. Conditions on milling operation can vary depending on whether it is: (i) a continuous process, where the size of the mill is the design parameter; or (ii) a batch process, where time is the design condition.

Population balance modeling (PBM) can be used for describing the rate of breakage of solids undergoing a milling process, and thus determining operation time or mill size in order to obtain a specific PSD [7]. This analysis presents an analogy with reactor design where the rate reaction of reactants and products is used to design reactors for a specific conversion [8]. It was originally proposed for particle aggregation processes [9] through the general Smoluchowski equation, to explain the process of coagulation and flocculation. For milling processes, it is applied to discretized particle sizes. The fundamental proposition states that the rate of breakage (r_i) of material from a sieve size to another follows a linear kinetic model [7]. That is, proportional to the mass of size i present in the mill and ignoring interactions with other sizes:

$$-r_i = k_i m_i \tag{1}$$

where m_i is the mass retained by mesh i and k_i is the breakage kinetic constant. For discretized intermediate sieve classes, this expression consists of an additional term corresponding to the mass of size i being produced by larger sizes. This is described as follows for a well-mixed milling process [10]:

$$-r_i = k_i m_i - \sum_{j=1}^{i-1} b_{ij} k_j m_j \tag{2}$$

where b_{ij} represents the fraction of material ground from sieve size j to size i and it is known as the breakage function. Figure 1 depicts this mechanism of breakage as an irreversible reaction in series, where the reactants and products are particles of different sizes. A fraction of a large size particle can break into a smaller size or to any other size, represented by the breakage function.

The rate of breakage for discretized particle sizes can be integrated into a mass balance for the size i for continuous (eq. 3) or batch (eq. 4) operation.

$$F_{i,in} - F_{i,out} = r_i M \tag{3}$$

$$\frac{dm_i}{dt} = -r_i M \tag{4}$$

where, $F_{i,in}$ and $F_{i,out}$ are respectively the mass flow of size i entering and leaving the mill; M the hold-up mass inside the mill and m_i is the mass fraction, Modeling a specific process consists of finding the values for k_i and b_{ij} through regression from experimental data.

PBMs have been widely used in studies of milling processes, for instance to explain the mechanisms of grinding [7, 11–14], the behavior of grinding media [15], scale-up of processes [6, 12, 16–19] and evaluate the predictability of these models [11,20, 21]. PBM may include energy consumption, feed rate, mill speed, fillings materials, and other parameters in order to improve the flexibility of the model for different applications [11, 14, 21].

Moreover, the grinding of solid blends is very common in industrial processes. For example, the addition of elements such as limestone, pozzolana, fly ash and slag to cement clinker can be made through an intergrinding process instead of grinding them individually and mixing them afterward [22]. This leads to a reduction in capital costs and produces finer particles due to synergetic interactions [23]. In mineral industries, extracted materials have several mineralogical components with different toughness and sizes, which may lead to non-optimal particle sizes and higher energy consumption [24]. This simplifies the process flowsheet, by combining milling and mixing, but may increase energy consumption. These interactions, which arise from the blending must be studied in order to determine its viability. This usually makes the modeling process more complicated and challenging.

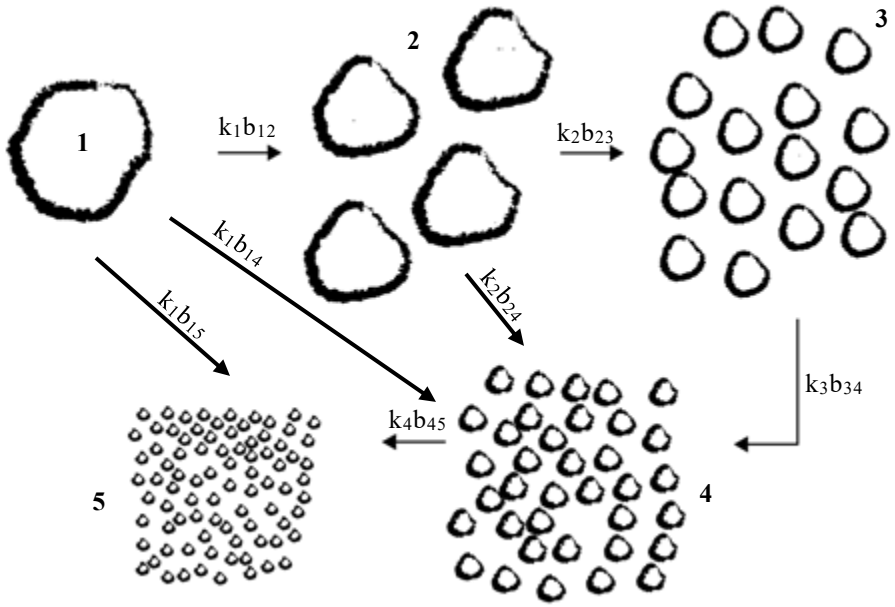

Figure 1. Breakage mechanism as explained by PBM.

These solid blends have not been largely studied, and there are few reports describing their behavior through dynamic models [17, 25–27]. These studies have explained the variation of materials breakage rate when milled alone and in a mixture; it increases for the weaker material and decreases for the stronger material. Theses variations also depend on the mass fraction of each component. Also, the energy consumed is distributed according to the mass fraction of each material. These results can be used with the methodology developed for single material for scale-up of processes and include other parameters to increase the model flexibility. However, the simulation applicability of the models is not verified through additional experimentation but with the same experimental data used for building the model. Moreover, the models developed are based on a mono-sized feed, which is not common in industrial processes and can alter the predictability of the model when using different PSD as feed.

Although there are many recent studies that describe the milling process using population balances, largely due to advances in computational methods and efficiency, studies involving modeling of milling of different materials at once have not evaluated the process in isolated scenarios, and so they may not be useful for the application in designing of equipment. Therefore, this project proposes to model blends in batch comminution operations using PBM, in order to evaluate its applicability in equipment design and PSD prediction based on random initial size distributions as a function of the operating time.

2. Materials and methods.

In this study, several experiments were made in a batch milling process for two materials and their blend. The experiments were made at the Unit Operations lab at EAFIT University. The solid materials used were ceramic waste from a toilet production process and chert, which is a mineral used in cement processing composed mainly of quartz (SiO_2). Two samples of each material were analyzed. For each run, the materials were screened through a 5/16 in aperture sieve in order to discard coarser particles. An in-house ball mill was used. Rotation speed and ball charge were kept constant for all experiments. The conditions for milling are shown in Table 1. According to specifications given by Ipek et al. [27], only 60% of the mill volume was considered for the operation. The mass for each material was determined as 50% of the effective mill volume, except for second sample of chert where mass was determined according to material availability. The fractional ball filling and the fractional material filling represent the volume occupied by the balls and the material in relation to the total effective mill volume, respectively. The electrical power driven to the mill was taken every

second for each experiment and then, using numerical integration, the total energy consumption for each interval of time was calculated. The density of the solids was determined in a test tube using liquid displacement.

The milling times were based on a geometric succession [18] with additional intermediate values. Thus, the sampling times were 0.5, 1.0, 2.0, 4.0, 8.0, 12.0, 16.0, 20.0 and 40.0 minutes. The experiments consisted of the evaluation of the PSD at these different milling times based on an initial distribution. PSD determination was made with a sieve series (Analytica Ltda.), with sieve numbers 4, 8, 10, 16, 30, 50, 100 and 200 according to ASTM E11 [28]. For each measurement, all the contained material in the ball mill was subject to screening in a ro-tap (Humboldt Mfg. Co.) for 10 minutes. An additional screening of 5 minutes was made for the fine fraction (sieves 50, 100, 200 and collector) in order to guarantee a better separation. After the analyses all the material was fed back into the mill to continue the size reduction process.

Table 1. Ball mill conditions, grinding media characteristics and material charge used in the milling process.

	Parameter	Value
Mill	Diameter (cm)	18.5
	Length (cm)	29.5
	Speed (rpm)	120
	Critical speed (rpm)	105.80
Grinding Media	Average diameter (mm)	25.11
	Number of balls	28
	Total mass (g)	1894.9
	Ball density (g/cm^3)	7.59
	Fractional ball filling	5.04%
	Average diameter (mm)	19.86
	Number of balls	60
	Total mass (g)	1840.7
	Ball density (g/cm^3)	8.13
	Fractional ball filling	4.96%
	Average diameter (mm)	16.83
	Number of balls	50
	Total mass (g)	914.5
	Ball density (g/cm^3)	9.54
	Fractional ball filling	2.09%
Material Charge	Fractional material filling	50%
	Ceramic 1 mass (g)	1025.7
	Ceramic 2 mass (g)	1008.1
	Chert 1 mass (g)	1001.0
	Chert 2 mass (g)	808.7

The retained mass in each sieve was normalized to the total feed mass. With each mass fraction, the differential and cumulative granulometric analyses were made [1]. The particle size for differential analysis was taken as the mean size between the sieve retaining the material and the previous sieve size. Particles were taken as spherical, that is, their form factor was equal to one.

Energy consumption was evaluated with the Charles energy size reduction equation [17]. This states the dependency of the specific energy E(kWh/ton) with size and distribution modulus (X_m and α, respectively) from the Gaudin-Schumann size distribution and a constant C, which corresponds to a particular material in a mill system:

$$E = CX_m^{-\alpha} \quad (5)$$

The size and distribution modulus are a representation of the desired PSD, and the value of C represents the grindability of the material. Thus, the higher the value of C, the lower the grindability of the material and more energy will be required to obtain a desired PSD. The Charles equation can be applied to mixtures of materials [27]:

$$E = m_1 C_1 X_{m1}^{-\alpha_1} + m_2 C_2 X_{m2}^{-\alpha_2} \quad (6)$$

where m_i is the mass fraction of each component. With this relationship, it was possible to determine the specific energy required to obtain given PSDs.

Initially, the model was adjusted with equation 2, taking the breakage function as one for the immediately previous size and zero for the other sizes. Thus, the only parameters present in the equations were the breakage constants (k_i). Therefore, a system of nine differential equations was obtained from the mass balances (one for each sieve size), with eight breakage constants. The smallest particle size, corresponding to the collector pan, is considered as not being further ground. The numerical method Runge-Kutta-Fehlberg (RKF45)[29] was used for solving each time interval, using initial approximations for k_i based on the plots of the distributions. Each time interval was solved independently, taking the initial PSD as the final distribution of the previous time. The predicted size distribution was then compared with the experimental one and the quadratic errors were calculated. The total sum of the errors was then minimized using the Excel Solver method Generalized Reduced Gradient (GRG) by modifying the k_i. In order to determine the fitness of the models, the Mean Absolute Errors (MAE, eq. 5) will be calculated for each mesh and the Maximum Absolute Error (MAX, eq. 6) for the whole model.

$$MAE = \sum_{i=1}^{n} \frac{|y_i - \hat{y}_i|}{n} \quad (7)$$

$$MAX = \max\,(y_i - \hat{y}_i) \quad (8)$$

where y_i is the experimental value, $\hat{y}_i$ the predicted value and n the total number of observations.

The PBM was made solely based on the results for the pure materials since they define the mixture, and no further adjustments were made to the model. The blend of the two materials was prepared with 70% in mass of ceramic and 30% of chert for a total of 997.7g. The blends were used to test the direct applicability of the individually fit models to predict the resulting PSD in blends.

For the validation of the models, one sample of ceramic material with 1018.6g and random initial PSD was ground for 10 minutes. Then its final PSD was determined, and the predictability was evaluated using the absolute errors between the estimated data and the experimental values. The same was applied to two samples of the mixture containing 70% in the mass of ceramic and the rest of chert, for a total of 1001.6g and 1015.1g of mass respectively.

3. Results and analysis.

3.1. PSD Analysis.

Densities for each material in every particle-size can be found in Figure 2. No large differences are noticed for different particle sizes for ceramic material. However, fine sizes of chert have a lower value for density, which may indicate the liberation of minerals which are present in the solid. Therefore, the presence of these minerals affects the density of small-sized particles.

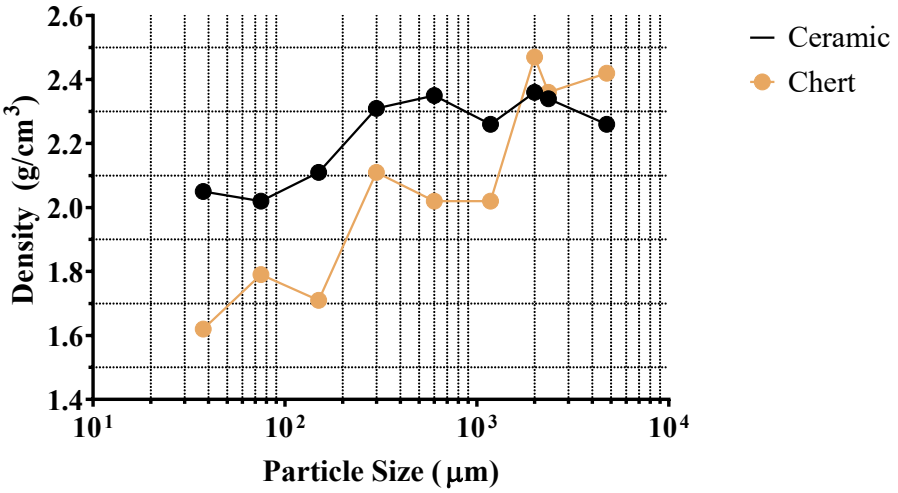

Figure 2. Density of ceramic and chert materials as functions of the particle size.

The power drawn by the mill was kept constant at a value of 128W. The Charles equations for ceramic and chert materials were determined as follows:

$$E_{Ceramic} = 8534X_m^{-0.8} \quad (9)$$

$$E_{Chert} = 9350X_m^{-1.4} \quad (10)$$

After 40 minutes of grinding, the size modulus for ceramic samples were 66 and 96 µm, for specific energies of 139 and 102 kWh/ton. For chert, the size modulus were 31 and 22 µm, for specific energies of 81 and 126 kWh/ton. These results show that chert has a higher grindability and therefore it is possible to obtain fine particle sizes with lower energy consumption than ceramic material.

Figure 3 shows the evolution of the retained mass fraction of each mesh for the two samples of the ceramic material. Both samples have initially a large fraction in the coarser particle sizes (meshes 4 and 8). The initial PSD for both samples were very similar, with around 80% of the material retained in the coarser sieve sizes, and the evolution of the PSD with time was also similar. These coarser sizes present a monotonous decreasing behavior. This is because these sizes have a higher probability of colliding with the grinding material and since they are the coarser sizes no new particles are created in that range of particle sizes. Mesh number 10 has very low mass fraction retained during the whole experiments and no accumulations are noticed. This may indicate that the impact breakage inside the mill represents low energy contacts, generating abrasion of large particles which produces another large particle and small-sized particles [30], as shown in Figure 4, and therefore few particles retained in mesh 10 are produced.

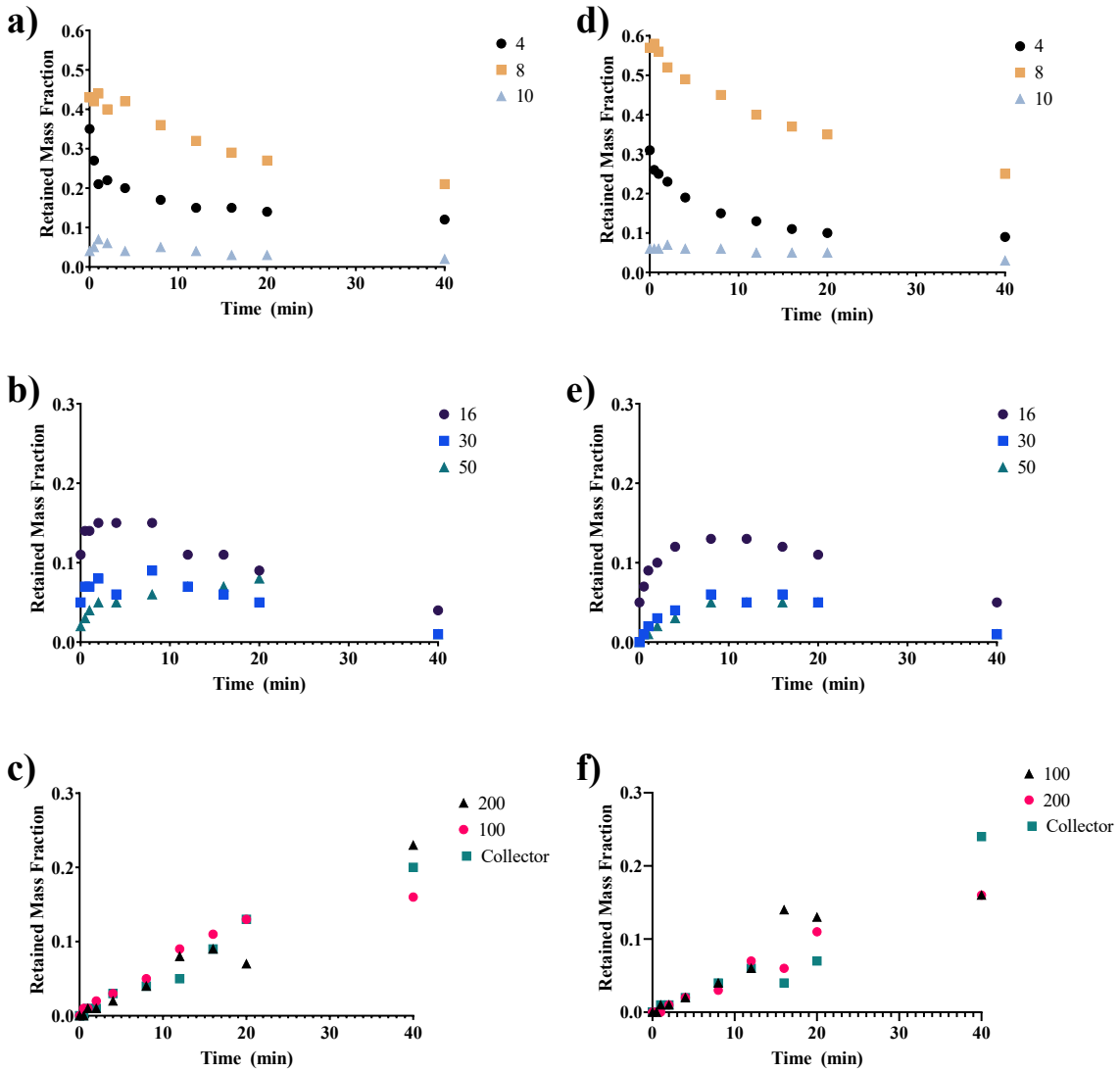

Figure 3. Retained mass fraction as function of time for both ceramic samples for each mesh: a) Ceramic 1 coarsest, b) Ceramic 1 intermediates, c) Ceramic 1 fines; d) Ceramic 2 coarsest, e) Ceramic 2 intermediates f) Ceramic 2 fines.

For intermediate sizes (mesh numbers 16, 30 and 50), retained mass fraction presents oscillations with time, and there are partial accumulations as shown by the convex graphs in Figures 2b and 2e. These accumulations occur when mass retained in mesh 8 has a larger value and therefore more material is being produced per time. After twelve minutes of grinding, the mass in intermediate sizes begins to decrease. At this time, material in smaller sizes breaks faster than they are being produced. These results match with the PBM assumption of the dependency of breakage rate with mass fractions.

Finer sizes (mesh numbers 100, 200 and collector pan) have a monotonous increasing behavior for both samples. This indicates a low value for the rate of breakage which ends up in accumulations in these sieve sizes. Also, the rate of production for these particle sizes is larger in later times. This can be attributed to the increasing rate of breakage of coarse and intermediate sizes.

Both chert samples have significantly different initial PSDs, as shown in Figure 5. For the first sample, a large amount of mass was retained in mesh numbers 4, 8 and 16, and the second sample had most of the mass retained in intermediate sieves, due to pregrinding.

The behavior of the particles being ground is very similar for both samples. Coarse and intermediate particle sizes exhibit a monotonic decreasing behavior (except for mesh 50 in Chert 1), indicating a fast rate of disappearance.

Finer sizes have an increasing behavior, indicating low values for the breakage rate. This also can be associated with the lower density for these particle sizes. However, the collector pan shows a high increase in the mass fraction in the later times, although mesh 200 shows an almost a steady fraction. This may indicate a series reaction where some of the coarser and intermediate sizes break into non-adjacent sieve sizes. A comparison between both materials in terms of evolution of mass fractions shows some similarities and differences. For coarser sizes, the mass fractions do not vary largely with time. Therefore, and despite the large mass fraction retained, the rate at which they disappear is not very high. Again, this can be explained as the process of abrasion, produced by the low energy impacts present in the ball mill, shown in Figure 4.

The similarities for both materials, in terms of high consumption for intermediate sizes, and low for coarser and finer sizes, can be attributed to the conditions of the milling process. The diameters for the milling media, in this case, steel balls, had a value that eased the breakage of intermediate sizes. These results reveal the necessity for the development of models accounting for other milling conditions, such as the characteristic for the milling media, rotation speed and milling time, which allow a better design of equipment in order to increase or decrease the breakage rate constant for certain sizes and to obtain the desired PSD [5, 21]. Also, mixing different solid materials can vary the breakage rate of some particle sizes [25], allowing them to have better selectivity for certain sizes.

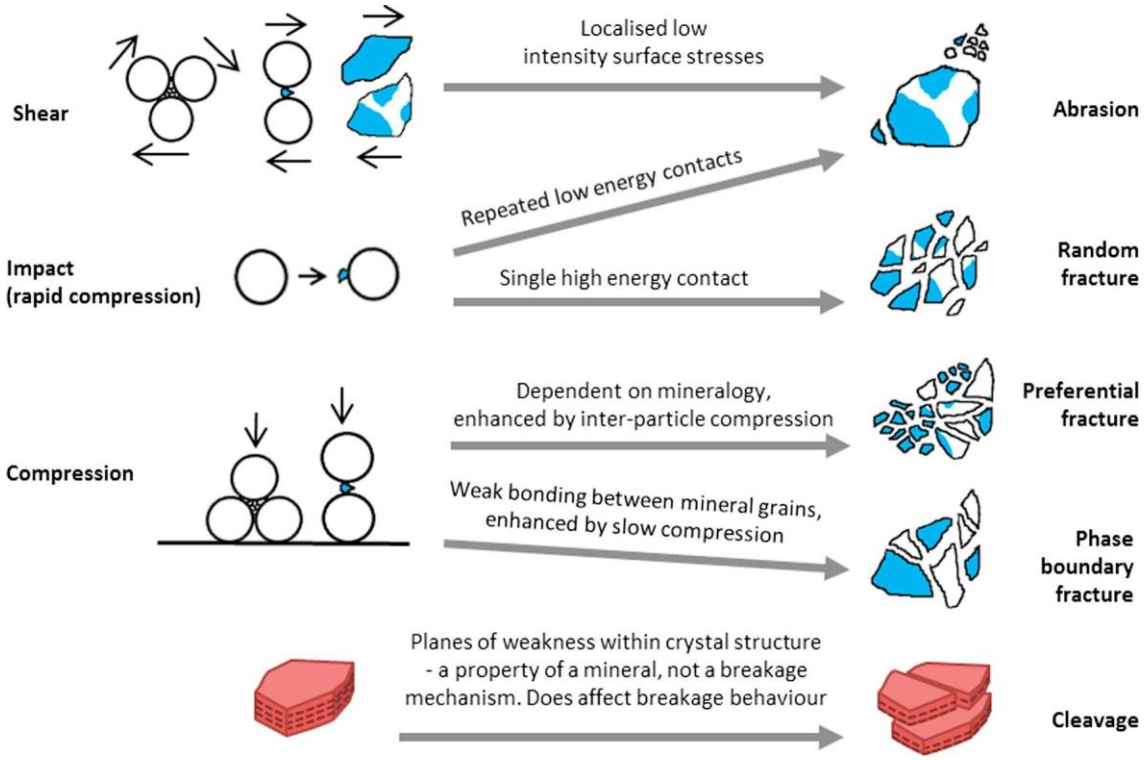

Figure 4. Breakage mechanisms. Source: Little et al. [30].

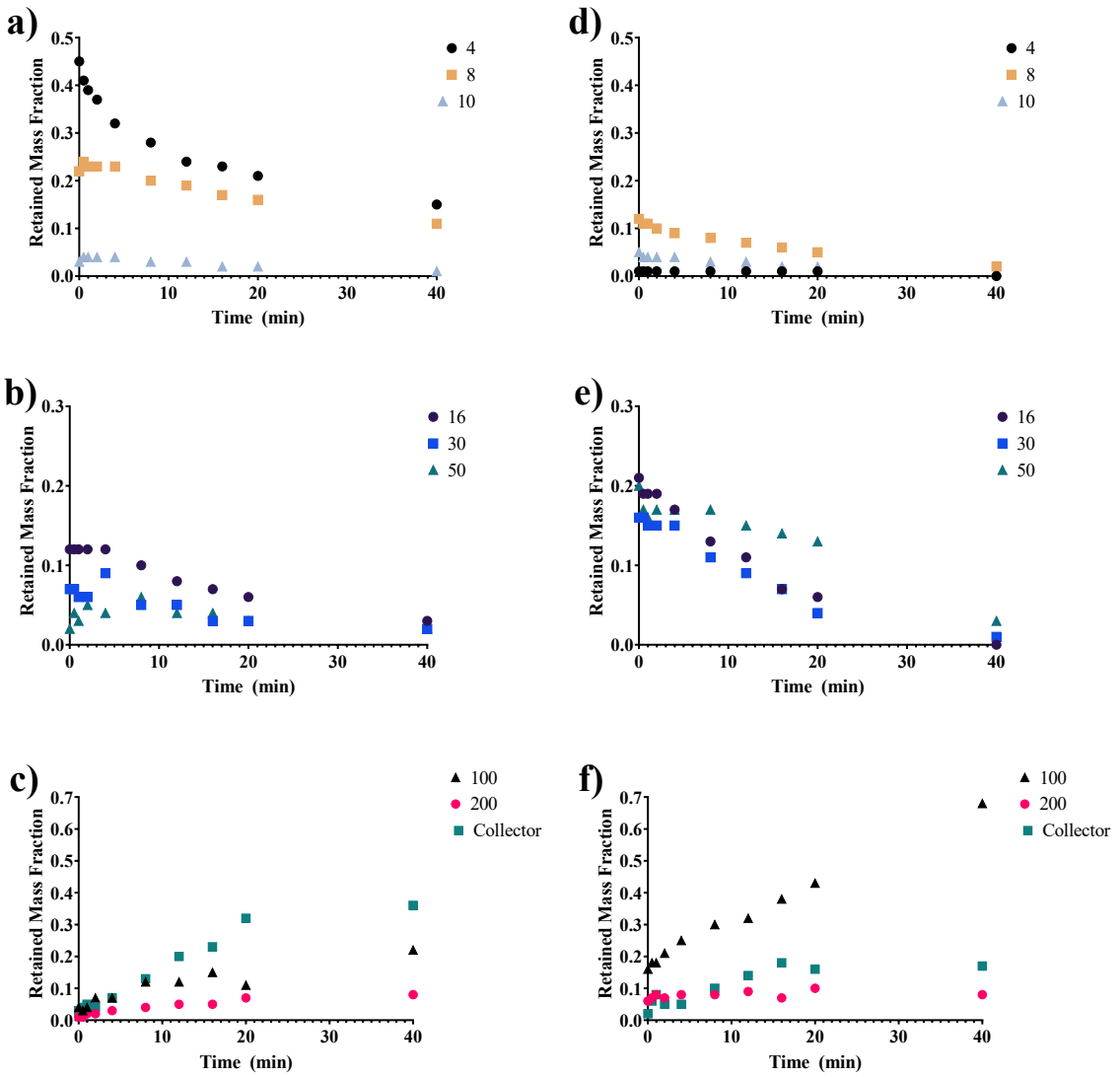

Figure 5. Retained mass fraction as function of time for both chert samples for each mesh: a) Chert 1 coarse sizes, b) Chert 1 intermediate sizes, c) Chert 1 fine sizes; d) Chert 2 coarse sizes, e) Chert 2 intermediate sizes, f) Chert 2 fine sizes.

3.2. Model fitting.

3.2.1. Model with no breakage function.

For this model, particles being ground are considered to produce only particles retained in the next sieve size. Thus, no material ground from one mesh to a non-adjacent mesh is considered. Breakage rate constants for each sieve size are reported in Table 2 for each material. These constants represent the linear dependency between breakage rate and mass fraction of each material. Both samples of each material were fitted into a single model in order to obtain the parameters for each particle size in the material. The collector pan constant is not considered since it is produced by mesh 200 but is not ground to finer sizes.

Table 2. Breakage rate constants for each sieve size for ceramic and chert materials.

	Breakage Rate Constant (min^{-1})	
Mesh	**Ceramic**	**Chert**
4	0.0531	0.0334
8	0.0489	0.0631
10	0.4759	0.2182
16	0.1603	0.1134
30	0.3138	0.1588
50	0.3092	0.1309
100	0.0989	0.0172
200	0.0625	0.1317

Values for the rate constants of coarse size, (sieves 4 and 8), are relatively low in comparison with those of intermediate sizes for all samples. The fracture of these particles, with the impact breakage present in the ball mill, might be producing particles of same size interval and therefore the mass fraction decreases slowly with time. This behavior can be attributed to the number of balls in the mill as well as their size. The largest diameter of the grinding media used is not able to effectively ground large-sized particles and therefore their constant rate is low. The mean size for particles retained in mesh 4 is 6375 µm with respect to the 8000 µm of mesh of 5/16 in of aperture. Larger balls had a diameter of 25 mm, which is almost four times larger. However, this difference was not enough for the effective grinding of this material. Then, according to the stress intensity[31], a larger ball diameter is required in order to increase the breakage constant for bigger particles at the given milling conditions. To determine this size, it is necessary to study the variation of PSD with specific energy, stress and different grinding media characteristics [5].

For the ceramic material, the results show a larger value for k_i for intermediate sizes. The evolution with time shows this behavior since mesh 10, for instance, does not accumulate with time. Mesh 16 shows some higher values in mass fraction due to slower grinding rate. Meshes 30 and 50 show a high and similar value for the rate constant, due to the presence of medium diameter balls, which eases their grinding. However, mass retained in mesh 30 decreases faster due to the low breakage rate form sieve 16. The highest values of mass fractions in this mesh may occur due to the high production from mesh 10 because of is high rate constant and initial mass fraction. Because of this, it might be necessary to include the breakage function to determine the amount of mass ground to non-adjacent sieve sizes. Finally, the finest sizes (sieves 100, 200 and collector pan) are produced very quickly from sizes 30 and 50 but they are not easily ground because of the high energy required to reduce small particles [30], and this is shown by the lower breakage constant rates.

The general model for the ceramic material shows variations mainly in sieves 30 and 50 as well. The consideration of additional parameters may reduce the differences and determine the dependency with initial PSD of the model.

Chert material shows the same behavior as the ceramic sample, except for last breakage constant, which is as large as those of the intermediate sizes. This shows that production of fines for chert material is easier. Also, it explains the large values for mass fraction in mesh 100, due to its low breakage rate. The larger values relatives to the other sizes still correspond to mesh 10 and intermediate sizes, but they are smaller in relation to the ceramic material. This can be explained for the differences in density for intermediate particle sizes and therefore the higher specific energy required.

The experimental values and the fitted models are shown in Figure 6. Here, the mass fractions were divided into coarse sizes (4, 8 and 10), intermediate sizes (16, 30 and 50) and fine sizes (100, 200 and collector) instead of each individual mesh. For the ceramic material, it can be seen a good fit for the intermediate and the fine fractions, as the lines of the model lie close to the experimental data. However, the coarse fractions show deviations between the fitted and experimental values. Chert material shows a good fit for the second sample, and the mean errors shows main deviations in the fine fraction. This can be attributed to the harder separations of these particles sizes and then is better to explain the three sizes added. The first sample of chert shows more deviation for every fraction.

From Figure 7, the largest values for the error are for the coarse and fine mass fraction. The Maximum Absolute Errors are, respectively, 0.13, 0.13, 0.26 and 0.17 for Ceramic 1, Ceramic 2, Chert 1 and Chert 2. These large values, of more than 10% of mass fraction retained, are present in the coarser sizes, especially the mesh 4 and fine fractions. As mesh 4 show the largest value for every sample (except for chert 2, which had low mass of this size), a non-linear dependency for rate of breakage with retained mass fraction could be considered. Also, in order to improve the goodness of fit of the model, the breakage function can be considered. This might allow explaining the differences between mass consumed in coarser sizes and mass-produced in finer particle sizes.

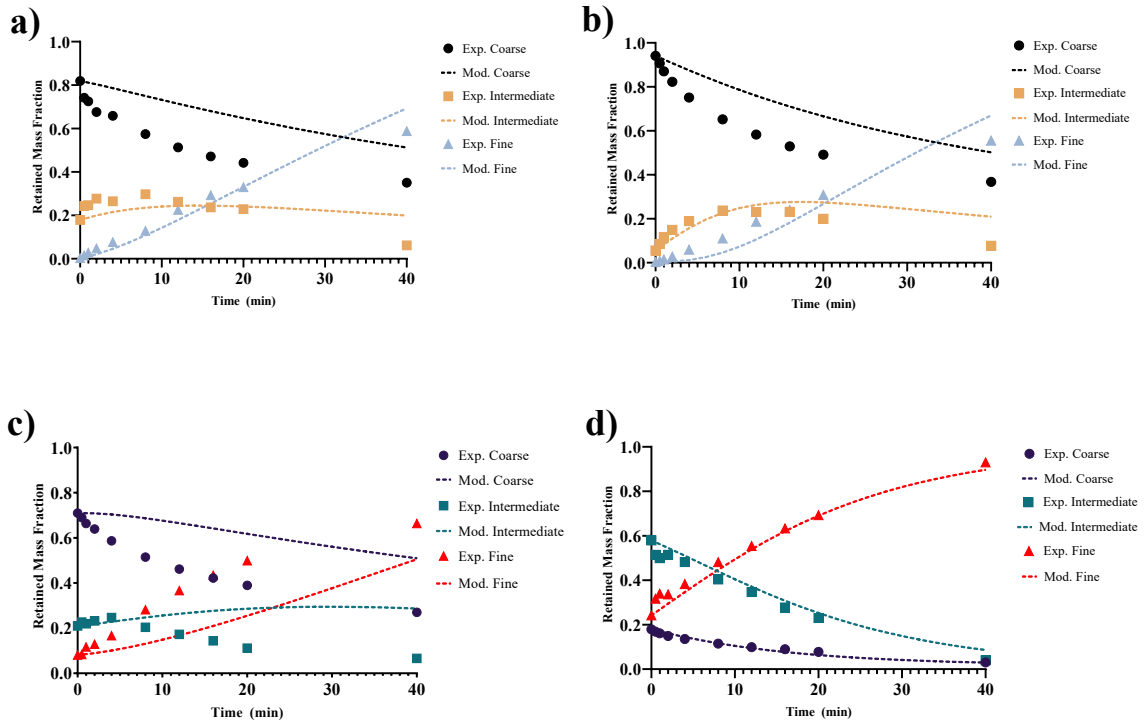

Figure 6. Retained mass fraction as function of time for coarse, intermediate and fine fractions for a) Ceramic 1, b) Ceramic 2, c) Chert 1, d) Chert 2. The dotted lines represent the adjusted models and points the experimental data.

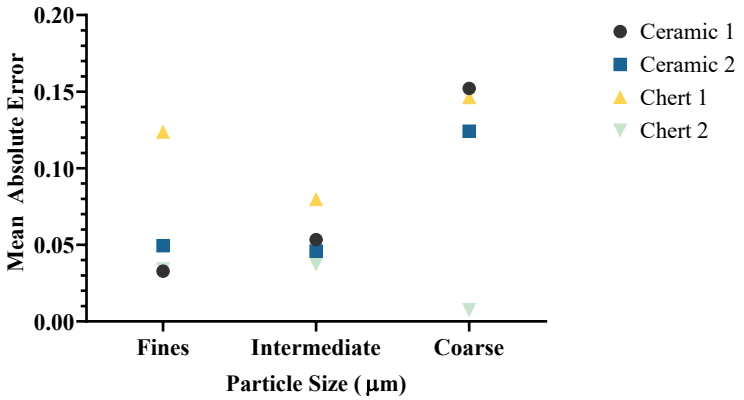

Figure 7. Mean absolute errors for the model without breakage function for each particle size for the four samples of ceramic and chert materials.

3.2.2. Model with breakage function.

For this model, additional terms (b_{ij} in equation (2) representing mass grinding from one size to a non-adjacent one were considered. Also, for mesh 4, a second-order dependence is considered. Tables 3 and 4 show the values for the breakage function and the breakage rate constant for the ceramic material and chert, respectively. For the breakage function, each number represents the fraction of mass ground from the mesh in the left column to the mesh in the second row. Some numbers are larger than unity because their effective value is multiplied with the breakage constant as seen in equation 2.

From these results, it is possible to determine the mechanisms implied in the milling process. For example, it can be seen a large amount of mass being ground from mesh 10 to mesh 16, which may account for the absence of accumulation and the high rate constant obtained with the previous model. Also, a larger value for the rate constant is found for mesh 4. This is product of the second-order dependency established and the breakage of this size to smaller sizes such as the mesh 16 and 30. Accumulations in earlier times may be attributed to this fact. The breakage rate constant still presents a high value for mesh 30, but it is lower for meshes 10 and 50. However, this value gets compensated with the breakage function which present high values for both, indicating their high breakage rate. Mesh 16 shows a higher value for the breakage rate, but the low values for the breakage function explain the accumulation observed in the evolution figures (Tables 3 and 4).

Table 3. Breakage rate constant and breakage function for the model fitting of ceramic material.

	Breakage function								Breakage Rate
	8	10	16	30	50	100	200	Collector	Constant (min^{-1})
4	0.02	0.00	0.14	0.18	0.09	0.03	0.01	0.02	0.3936
8		0.48	0.05	0.75	0.09	0.01	0.01	0.11	0.0254
10			1.98	0.21	0.4	0.56	0.63	0.10	0.1491
16				0.06	0.22	0.04	0.01	0.01	0.1531
30					0.04	0.08	0.01	0.03	0.2772
50						0.10	0.16	0.22	0.1690
100							0.46	0.12	0.0169
200								0.49	0.0006

Table 4. Breakage rate constant and breakage function for the model fitting of chert material.

	Breakage function								Breakage Rate
	8	10	16	30	50	100	200	Collector	Constant (min^{-1})
4	0.11	0.00	0.03	0.00	0.01	0.00	0.02	0.10	0.2082
8		0.10	0.04	0.13	0.14	0.01	0.08	0.16	0.0461
10			4.09	0.26	0.48	1.22	0.27	0.08	0.0798
16				0.09	0.24	0.05	0.02	0.01	0.1338
30					0.08	0.11	0.01	0.05	0.0809
50						0.96	0.04	0.60	0.0750
100							1.19	0.34	0.0000
200								0.50	0.0005

Figure 8 shows a better fit of the value generated with the model with the experimental data. Also, mean absolute errors show a better approximation of the estimated to the experimental data, as shown in Figure 9. Assuming a second-order kinetic for the coarsest size, the error decreases. Second-Order kinetic consists of particles of the same size colliding against each other for their grinding. When mass fraction decreases, so do the breakage rate. This explains the more adequate fitting of this model. However, fine and coarse fractions still present larger errors with respect to the intermediate. Also, Maximum Absolute Errors are 0.11, 0.24, 0.11, 0.12 for Ceramic 1, Ceramic 2, Chert 1 and Chert 2, respectively, which are lower values, but they still represent around 10% of mass retained of difference with respect to experimental values. Further analysis can be made in order to improve the fit of the model, such as the effect of grinding media of other orders of reaction. For example, it can be considered the mechanism of attrition for coarse sizes; thus, the order would be zero since

particles of same size are being produced. Similarly, for fine sizes, it can be considered the loss of material through the experiments including a hold-up term. However, the model is suitable for the materials studied and will be used to the evaluation of their blend.

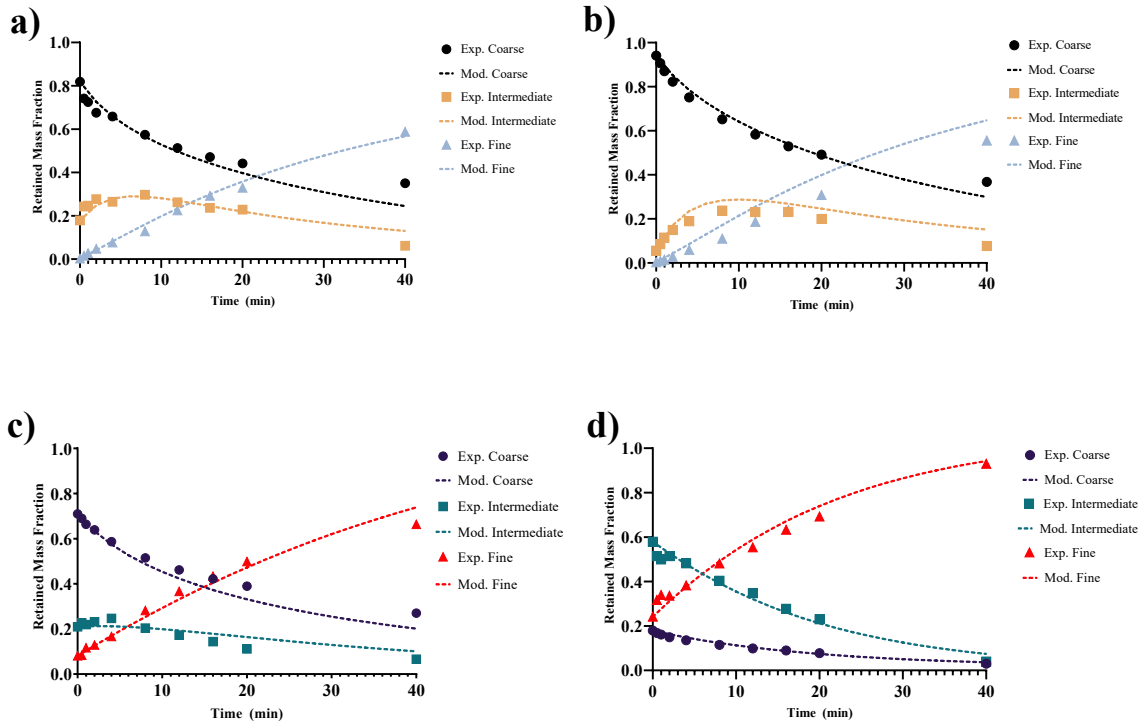

Figure 8. Retained mass fraction as function of time for coarse, intermediate and fine fractions for a) Ceramic 1, b) Ceramic 2, c) Chert 1, d) Chert 2. The dotted lines represent the model including b_{ij} and points the experimental data.

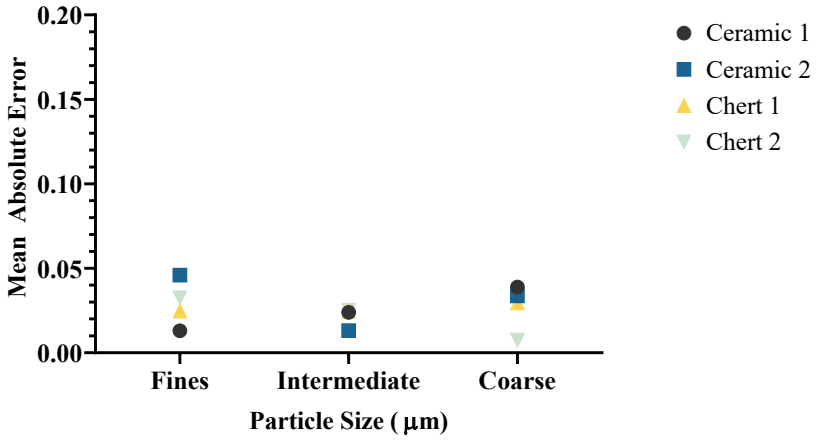

Figure 9. Mean absolute errors for each particle size for the four samples of ceramic and chert materials for the model with b_{ij}.

3.2.3. Blend model.

According to results obtained for pure materials, PBM for the blend of the materials was evaluated using the parameters for the model of each material. The values for the breakage rate constant (k_i in equation 2) and the breakage function (b_{ij} in equation 2) were calculated as the linear combination, taking the mass fraction of each

component, that is, 0.7 for ceramic and 0.3 for chert. This relation is essentially the same in volume fraction due to similarities in density for both materials.

Figure 10 shows the evolutions with time of the coarse, intermediate and fine sizes fractions for the blend. It can be seen that the data is not being explained by the model. The coarse fraction is being overestimated since the rate of breakage of the model is lower than the actual. On the contrary, the intermediate sizes and the finest sizes have lower values predicted by the model. Mean absolute errors, shown in Figure 11 for each particle size, show the lack of fit especially for the collector and the fine fraction. These results imply that the resulting parameters of the model in a mixture, for a milling process, is not the lineal combination of the parameters of the pure components. This behavior can be attributed to synergies generated when mixing the materials and therefore the linear model is not able to capture the differences.

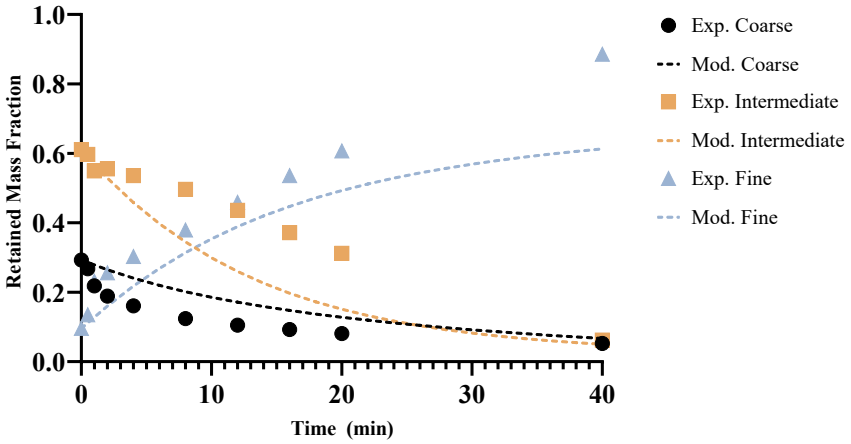

Figure 10. Retained mass fraction as function of time for coarse, intermediate and fine fractions for the blend of 70% of Ceramic and 30% of Chert in mass. The dotted lines represent the model and points the experimental data.

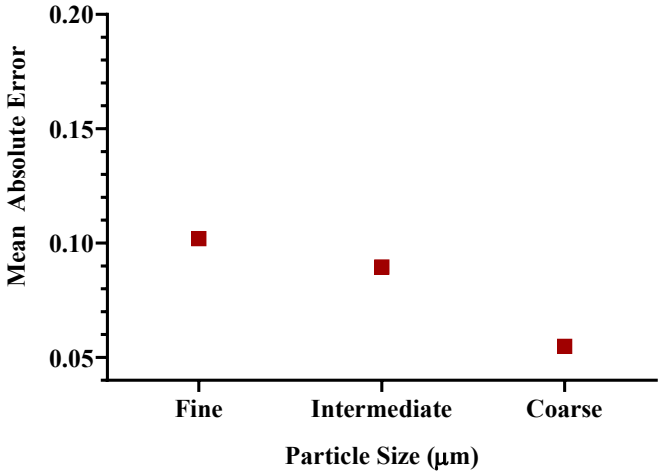

Figure 11. Mean absolute errors for each particle size for the blend of 70% of ceramic and 30% of chert in mass.

The sum of mass fractions in some grinding times is not equal to 1, as seen after 40 minutes of grinding. This is due to the independency in the prediction of each particle size. The normalization of the data can be coerced in order to solve this problem. In this case, the fit for the fine mass fractions improves but coarse and intermediate sizes are still not explained by the model, as shown in Figure 12.

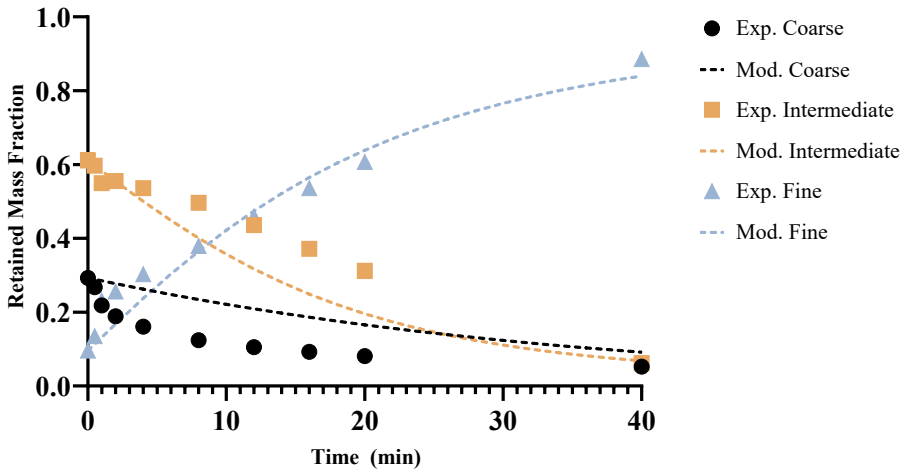

Figure 12. Retained mass fraction as function of time for coarse, intermediate and fine fractions for the blend of 70% of Ceramic and 30% of Chert in mass. The dotted lines represent the normalized model and points the experimental data.

3.3. Model evaluation.

Additional experiments with random initial PSD were made in order to evaluate the predictability of the fitted models. Table 5 shows the initial PSD as the experimental and predicted PSD for a ceramic sample after 10 minutes of grinding. It is possible to see that fine size fractions are predicted accurately while coarse and intermediate fractions present large variations between the experimental value and the fitted value. The adjusted parameters are unable to capture the changes in behavior of different initial PSDs. Therefore, additional experiments must be made in order to account for other parameters or more initial PSDs.

Table 5. Retained mass fractions for coarse, intermediate and fine sizes for ceramic model validation.

	Retained Mass Fraction		
	Coarse	Intermediate	Fine
Experimental	0.26	0.47	0.28
Predicted	0.36	0.33	0.31

The experiments involving the blend of the material, and the PBM developed, do not show a good approximation to the experimental data. The predicted values in Table 6 show large differences for intermediate sizes, but similar values for the coarse and fine fraction. Moreover, these results are not reliable and should not be used for predicting PSD. It is necessary to study the relation between mass fraction of each component and the parameters of the models in order to establish adequate values for their blend.

Table 6. Retained mass fractions for coarse, intermediate and fine sizes for blend model validation.

	Retained Mass Fraction					
	Blend 1			Blend 2		
	Coarse	Intermediate	Fine	Coarse	Intermediate	Fine
Experimental	0.26	0.47	0.28	0.25	0.36	0.40
Predicted	0.16	0.41	0.43	0.30	0.24	0.46

Conclusions.

Results obtained from the PBM allowed to explain the variation of PSD with time for a ceramic material and chert. The values for the breakage constants and breakage function showed that abrasion occurred for coarser sizes and fracture for intermediate and fine sizes.

The breakage rate of coarse particles was not successfully fitted using a linear kinetic expression. Therefore, a second order kinetic was used instead, which presented better approximations. This was because of the low size of grinding media used in the experiments. Further work should be focused on determine the influence of grinding media in PBM in order to maintain the linear relation.

Evaluation of the models showed significant variations when the prediction of PSD was intended. The absolute errors were around 20% in mass fraction for coarse and intermediate particle sizes. However, mass fractions of the finest particles show variations of only 2%. More robust adjustments are required in order to improve the applicability of PBM to grinding processes.

In the study of solid blends, it was not possible to establish a dependence of the PBM parameters with those of the pure component behavior. Besides, it was not possible to predict the final PSD using a PBM relation initial particle size distribution with milling time, due to the presence of errors of above 10% in mass fraction.

Annexes and appendixes table

Table 7. Additional documents included with the project.

Name	Development	File type	Google drive URL
Evolution of PSD with time for pure materials and their blend	Own	PDF	shorturl.at/cnuY8

References

[1] W. L. McCabe, J. C. Smith, and P. Harriot, *Unit Operations of Chemical Engineering*, 5th ed. International Editions, 1993.

[2] J. P. Liévano, J. C. Thomas, R. Molano, E. H. Valero, and B. C. Ramírez, "Comportamiento de las 1.000 empresas más grandes del sector real, por ingresos operacionales. Informe," 2019.

[3] J. Bouchard, A. Desbiens, and É. Poulin, "Reducing the energy footprint of grinding circuits: the process control paradigm," *IFAC-PapersOnLine*, vol. 50, no. 1, pp. 1163–1168, 2017.

[4] M. Hacksteiner, H. Peherstorfer, and F. Bleicher, "Energy efficiency of state-of-the-art grinding processes," in *Procedia Manufacturing*, 2018, vol. 21, pp. 717–724.

[5] R. Perry and D. Green, "Perry's Chemical Engineers' Handbook," *McGraw-Hill, New York*, p. 2234, 1997.

[6] V. K. Gupta, "An appraisal of the energy-size reduction relationships for mill scale-up design," *Adv. Powder Technol.*, vol. 30, no. 1, pp. 73–84, Jan. 2019.

[7] E. Guasch *et al.*, "New approach to ball mill modelling as a piston flow process," *Miner. Eng.*, 2018.

[8] M. E. Davis and R. J. Davis, *Fundamentals of chemical reaction engineering*. McGraw-Hill, 2003.

[9] R. I. Jeldres, P. D. Fawell, and B. J. Florio, "Population balance modelling to describe the particle aggregation process: A review," *Powder Technology*, vol. 326. Elsevier B.V., pp. 190–207, 2018.

[10] L. G. Austin, "Introduction to the mathematical description of grinding as a rate process," *Powder Technology*, vol. 5, no. 1. pp. 1–17, 1971.

[11] L. G. Austin, C. A. Barahona, and J. M. Menacho, "Investigations of Autogenous and Semi-Autogenous Grinding in Tumbling Mills," *Powder Technology*, vol. 51. pp. 283–294, 1987.

[12] V. K. Gupta, "Understanding production of fines in batch ball milling for mill scale-up design using the population balance model," *Adv. Powder Technol.*, vol. 29, no. 9, pp. 2035–2047, 2018.

[13] S. L. A. Hennart, W. J. Wildeboer, P. van Hee, and G. M. H. Meesters, "Identification of the grinding mechanisms and their origin in a stirred ball mill using population balances," *Chem. Eng. Sci.*, vol. 64, no. 19, pp. 4123–4130, 2009.

[14] S. Nomura, "Analysis of holdups in continuous ball mills," *Powder Technol.*, vol. 235, pp. 443–453, 2013.

[15] I. Rivera, F. Quintero, O. Bustamante, and G. Loaiza, "Aplicación de un modelo de balance poblacional a un molino de bolas en la industria del cemento," *Ing. y Cienc.*, vol. 10, no. 19, pp. 163–177, 2014.

[16] K. G. Tsakalakis and G. A. Stamboltzis, "Modelling the specific grinding energy and ball-mill scaleup," in *IFAC Proceedings Volumes (IFAC-PapersOnline)*, 2004, vol. 37, no. 15, pp. 53–58.

[17] K. S. Venkataraman and D. W. Fuerstenau, "Application of the population balance model to the grinding of mixtures of minerals," *Powder Technol.*, vol. 39, no. 1, pp. 133–142, 1984.

[18] J. A. Herbst and D. W. Fuerstenau, "Scale-up procedure for continous grinding mill design usign population balance models," *International Journal of Mineral Processing*, vol. 7, no. 1. pp. 1–31, 1980.

[19] M. Capece, "Population balance modeling applied to the milling of pharmaceutical extrudate for use in scale-up," *Adv. Powder Technol.*, vol. 29, no. 12, pp. 3022–3032, 2018.

[20] L. M. Tavares, "A review of advanced ball mill modelling," *KONA Powder and Particle Journal*, vol. 2017, no. 34. Hosokawa Powder Technology Foundation, pp. 106–124, 2017.

[21] A. L. R. de Oliveira and L. M. Tavares, "Modeling and simulation of continuous open circuit dry grinding in a pilot-scale ball mill using Austin's and Nomura's models," *Powder Technol.*, vol. 340, pp. 77–87, 2018.

[22] S. Tsivilis, N. Voglis, and J. Photou, "Study on the intergrinding of clinker and limestone," *Miner. Eng.*, vol. 12, no. 7, pp. 837–840, 1999.

[23] A. Arora, K. Vance, G. Sant, and N. Neithalath, "A methodology to extract the component size distributions in interground composite (limestone) cements," *Constr. Build. Mater.*, vol. 121, pp. 328–337, 2016.

[24] L. M. Tavares and R. D. C. Kallemback, "Grindability of binary ore blends in ball mills," *Miner. Eng.*, vol. 41, pp. 115–120, 2013.

[25] R. Zhao, Y. Han, M. He, and Y. Li, "Grinding kinetics of quartz and chlorite in wet ball milling," *Powder Technol.*, vol. 305, pp. 418–425, Jan. 2017.

[26] H. Cho and P. T. Luckie, "Investigation of the Breakage Properties of Components in Mixtures Ground

in a Batch Ball-and-Race Mill," *Energy and Fuels*, vol. 9, no. 1, pp. 53–58, 1995.
[27] H. Ipek, Y. Ucbas, and C. Hosten, "Ternary-mixture grinding of ceramic raw materials," *Miner. Eng.*, vol. 18, no. 1, pp. 45–49, Jan. 2005.
[28] ASTM, "U.S.A. Standard Sieves ASTM Specification E-11," *Astm E11-17*. 2017.
[29] "Runge-Kutta and Extrapolation Methods," in *Solving Ordinary Differential Equations I*, Berlin, Heidelberg: Springer Berlin Heidelberg, pp. 129–353.
[30] L. Little, A. N. Mainza, M. Becker, and J. Wiese, "Fine grinding: How mill type affects particle shape characteristics and mineral liberation," *Miner. Eng.*, vol. 111, pp. 148–157, 2017.
[31] M. Becker, A. Kwade, and J. Schwedes, "Stress intensity in stirred media mills and its effect on specific energy requirement," 2001.